Molecular Diversity (2021) 25:1701–1715
https://doi.org/10.1007/s11030-020-10136-9

ORIGINAL ARTICLE

Understanding the enzymatic inhibition of intestinal alkaline phosphatase by aminophenazone-derived aryl thioureas with aided computational molecular dynamics simulations: synthesis, characterization, SAR and kinetic profiling

Asma Khurshid[1] · Aamer Saeed[1] · Zaman Ashraf[2] · Qamar Abbas[3] · Mubashir Hassan[4]

Received: 9 May 2020 / Accepted: 19 August 2020 / Published online: 29 August 2020

Abstract

The work presented in this paper aims toward the synthesis of aryl thiourea derivatives **4a**–**l** of pyrazole based nonsteroidal anti-inflammatory drug named 4-aminophenazone, as potential inhibitors of intestinal alkaline phosphatase enzyme. The screening of synthesized target compounds **4a**–**l** for unraveling the anti-inflammatory potential against calf intestinal alkaline phosphatase gives rise to lead member **4c** possessing IC_{50} value 0.420 ± 0.012 µM, many folds better than reference standard used (KH_2PO_4 $IC_{50} = 2.8 \pm 0.06$ µM and L-phenylalanine $IC_{50} = 100 \pm 3.1$ µM). SAR for unfolding the active site binding pocket interaction along with the mode of enzyme inhibition based on kinetic studies is carried out which showed non-competitive binding mode. The enzyme inhibition studies were further supplemented by molecular dynamic simulations for predicting the protein behavior against active inhibitors **4c** and **4g** during docking analysis. The preliminary toxicity of the synthesized compounds was determined by using brine shrimp assay. This work also includes detailed biochemical analysis along with RO5 parameters for all the newly synthesized drug derivatives **4a**–**l**.

Electronic supplementary material The online version of this article (https://doi.org/10.1007/s11030-020-10136-9) contains supplementary material, which is available to authorized users.

✉ Asma Khurshid
asmakhurshid@chem.qau.edu.pk

✉ Aamer Saeed
aamersaeed@yahoo.com

[1] Department of Chemistry, Quaid-I-Azam University, Islamabad 45320, Pakistan

[2] Department of Chemistry, Allama Iqbal Open University, Islamabad 44000, Pakistan

[3] Department of Physiology, University of Sindh, Jamshoro, Pakistan

[4] Department of Molecular Biology and Biotechnology, The University of Lahore, Lahore, Pakistan

Graphic abstract

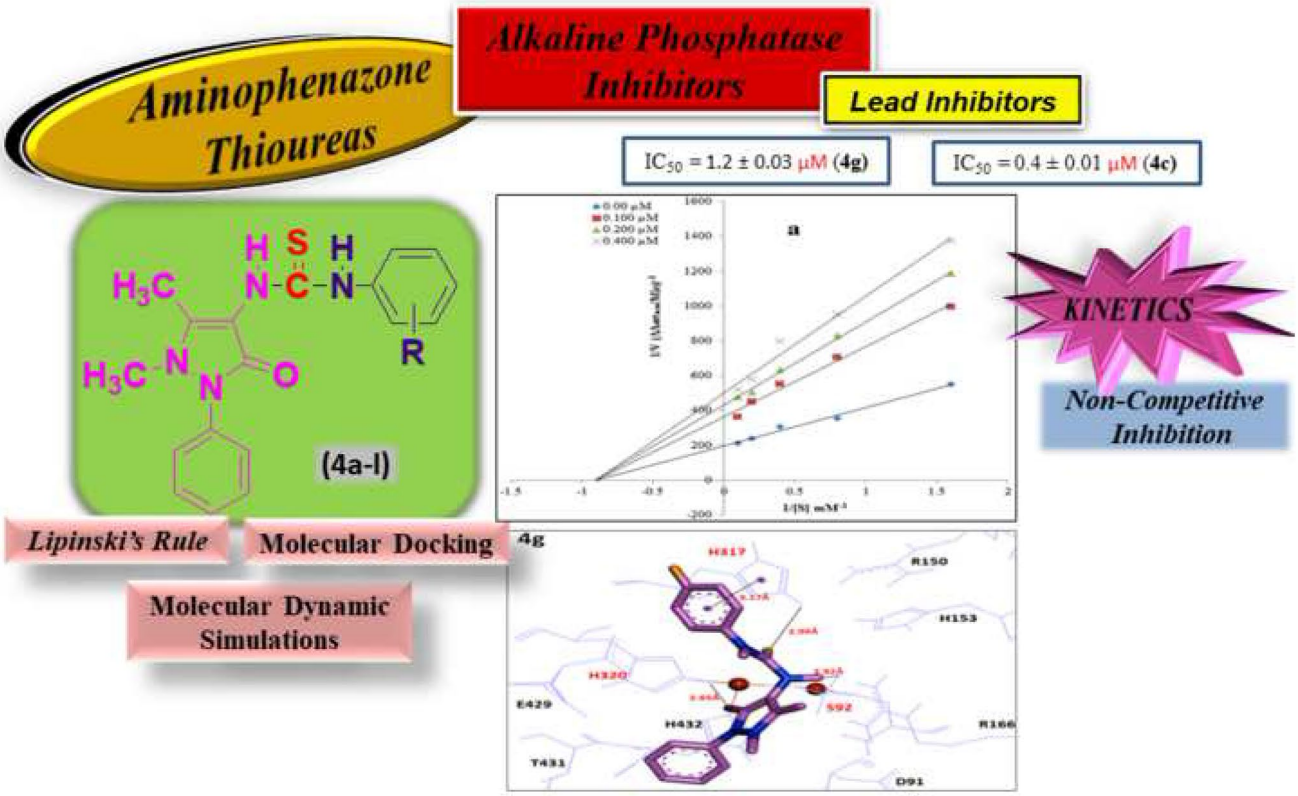

Keywords Aminophenazone · Intestinal alkaline phosphatase · Non-competitive inhibition · RO5 validation

Introduction

Alkaline phosphatase is a subdivision of the major class of ectoenzymes named as ectonucleotidases. These ectoenzymes are mainly involved in hydrolysis of extracellular nucleotides to nucleosides and adenosine via direct or indirect pathways. Alkaline phosphatases are found on the outer surface of plasma membrane and are responsible for catalyzing the hydrolysis of phosphate groups from a variety of different substrates (dephosphorylation) in an alkaline environment, freeing inorganic phosphate (Pi) [1, 2]. In addition to this, APs also mediate the hydrolysis of a variety of substrates other than nucleotides, such as bis(*p*-nitrophenyl) phosphate, inorganic polyphosphates, phosphatidates and glucose-phosphates [3].

There are four isozymes of alkaline phosphatases that are found in humans which include tissue non-specific AP (TNAP), germ cell AP (GCAP), placental AP (PLAP) and intestinal AP (IAP) [4]. The TNAP is tissue non-specific and can be found in liver, kidney and most abundantly in bones, while rest of three are tissue-specific isozymes and have relative homologies in the range of 90–98% with their genes clustered on chromosome 2, whereas the gene of TNAP is located on chromosome 1 and it is only 50% identical to the other three isozymes.

The function of TNAP varies according to the type of tissue where it is expressed. Mainly, it is associated with bone and tooth deposition processes and is anchored to the cell membranes of osteoblasts and chondrocytes, where it degrades PPi to Pi. PPi acts as an inhibitor of mineralization [5] and regulation by TNAP hence propagates the extracellular mineralization of apatite crystals. The deficiency of TNAP enhances the amount of inhibitory PPi and thus decreases the extracellular mineralization and humans suffering from hypophosphatasia (HPP) depict the loss of mineralization fronts [6]. The loss of mineralization is associated with various symptoms such as softening spontaneous breakage of bones, rickets and tooth (cementum/dentin/enamel) defects [7].

The biological function of tissue-specific PLAP is still unknown [8] and it resides in placental tissues. However, it is often observed in serum of patients with primary testicular tumors seminoma [9] and other cancers [10]. It has been reported that switching of genes from PLAP to GCAP may

lead to transformation from normal to malignant trophoblast since both PLAP and GCAP are co-expressed in ovarian cancers [11].

The third important type of tissue-specific alkaline phosphatase is intestinal alkaline phosphatase (IAP) that is expressed in villus-associated enterocytes and regulates fatty acid absorption at both the luminal and basolateral surfaces via secretion of vesicles [12, 13]. In addition, the IAP also regulates the duodenal surface pH [14] and bicarbonate secretion and is involved in the processes like diet-induced obesity [15, 16] and metabolic syndrome [17, 18]. But among all these functions, one of the most remarkable functions of IAP centers on its protective interactions with the bacterial symbionts that inhabit or invade our enteric system. With increasing research in microbiome physiology, the intestinal alkaline phosphatase (IAP) has become an immense core of interest to scientists due to its interaction with endogenous microbes and thus its ultimate influence on human health. In the literature, various intestinal alkaline phosphatase inhibitors such as L-phenylalanine, L-homoarginine, L-phenylalanineglycylglycine, L-leucine and levamisole have been reported that are used as standard drugs against intestinal alkaline phosphatase with varying inhibition ranges. However, it was found that among all the aforementioned inhibitor molecules, L-phenylalanine turns out to be the most active inhibitor specifically against intestinal alkaline phosphatase enzyme [19].

Considering the significant role of alkaline phosphatases, typically the intestinal alkaline phosphatases in maintaining balanced homeostasis in humans, there is a dire need to develop more effective and potent inhibitors/activators of intestinal alkaline phosphatases, so, as to cope with various health disorders originating due to under or over production of intestinal alkaline phosphatases [20].

Thioureas are an important class of organic compounds with longstanding interest in medicinal industry. They have been well documented in the literature for their astounding biomedical properties including antiparasitic, antifungal, antibacterial [21], anticancer, anti-HIV activities, antioxidant, urease inhibition, carbonic anhydrase inhibition, butyrylcholinesterase and acetylcholinesterase inhibition [22].

Due to their broad term medicinal potential, continued efforts are still in progress by scientific community in design and development of more effective thiourea derivatives with enhanced pharma effects. Various synthetic approaches such as microwave, ultrasonic-assisted approaches besides the traditional synthetic strategies have been utilized to access thiourea functionality [23–30].

The presence of fascinating structural features in thiourea such as free N–H atoms offers wide possibility for design and development of an array of heterocyclic scaffolds. In addition, the carbonyl and thiocarbonyl functionalities provide sites for chelation, thereby, serving as useful ligands in complexation chemistry [31, 32].

Additionally, thioureas serve as a useful alkaline phosphatase inhibitors with potential against various diseases like inflammation, cancer and cardia diseases. Some representative reported examples of such thioureas are highlighted in Fig. 1 [22, 33].

Among the broad range of nonsteroidal anti-inflammatory drugs, 4-aminophenazone also named antipyrine has got an immense importance in pharmaceutical industry due to its associated medicinal effects which includes

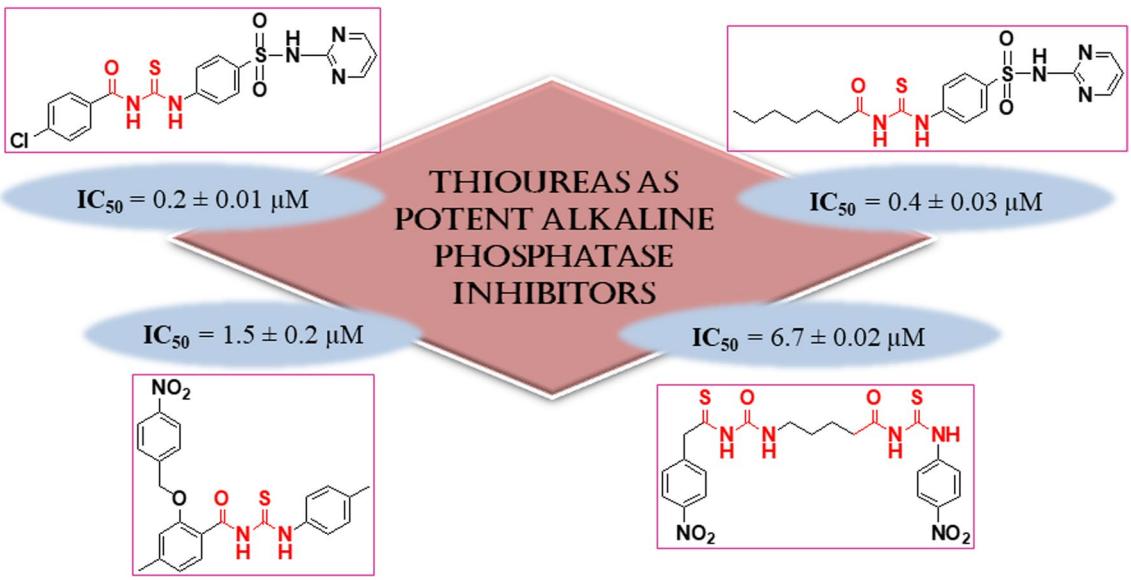

Fig. 1 Few examples of thioureas as potent intestinal alkaline phosphatase inhibitors

anti-pyretic, anti-inflammatory and analgesic effects [34]. It has also been known for its broad term use in therapies such as its application in treatment of soft tissue disorders, arthritis, neuralgia and lung inflammation, i.e., pneumonia [35]. Literature survey reveals the use of pyrazole based synthetic compounds by several research groups as active inhibitors against various enzymes such as nucleotide pyrophosphatase/phosphodiesterase, nucleoside triphosphatase diphosphohydrolase [36], protease-resistant prion protein [37] including various types of alkaline phosphatases [38], respectively.

In order to unfold the diversified biomedical potential of 4-aminophenazone by exploiting the effect of pyrazole nucleus as privileged pharmacophore in drug chemistry, we in past already reported aminophenazone-derived selective inhibitors [39]. With this continuation, taking into account, the broad range biomedical applications of thiourea functionality, the work presented in this paper is an extended effort toward synthesis of aminophenazone-derived aryl thioureas as significant inhibitors of alkaline phosphatases for treatment of various inflammation disorders including cancer diseases. The work is further supplemented by computational molecular dynamic simulation and enzyme inhibitory kinetic studies.

Results and discussion

Chemistry

Synthesis of target compound (**4a–l**) achieved via a multistep synthetic sequence is highlighted in Scheme 1. An equimolar quantity of carbon disulfide and ammonium hydroxide was added to a stirred solution of various suitably substituted anilines (**1a–l**) at low temperature (10 °C) and set to stirring for 12 h. This was followed by subsequent addition of aqueous solution of lead nitrate with additional stirring for overnight to form the corresponding substituted isothiocyanate intermediate **2a–l**. The freshly prepared pure isothiocyanate (**2a–l**) was then treated with 4-aminophenazone under reflux conditions to yield aminophenazone-based substituted aryl thiourea derivatives (**4a–l**) in good yields.

Spectroscopic characterizations

FTIR, $^{1}H/^{13}C$ NMR and elemental analysis (CHNS) have been used for structure elucidation of synthesized compounds (**4a–l**).

In case of FTIR, the formation of target compound **4a–l** is supported by appearance of characteristic stretching absorptions for NH bonds in the range of 3378–3169 cm^{-1},

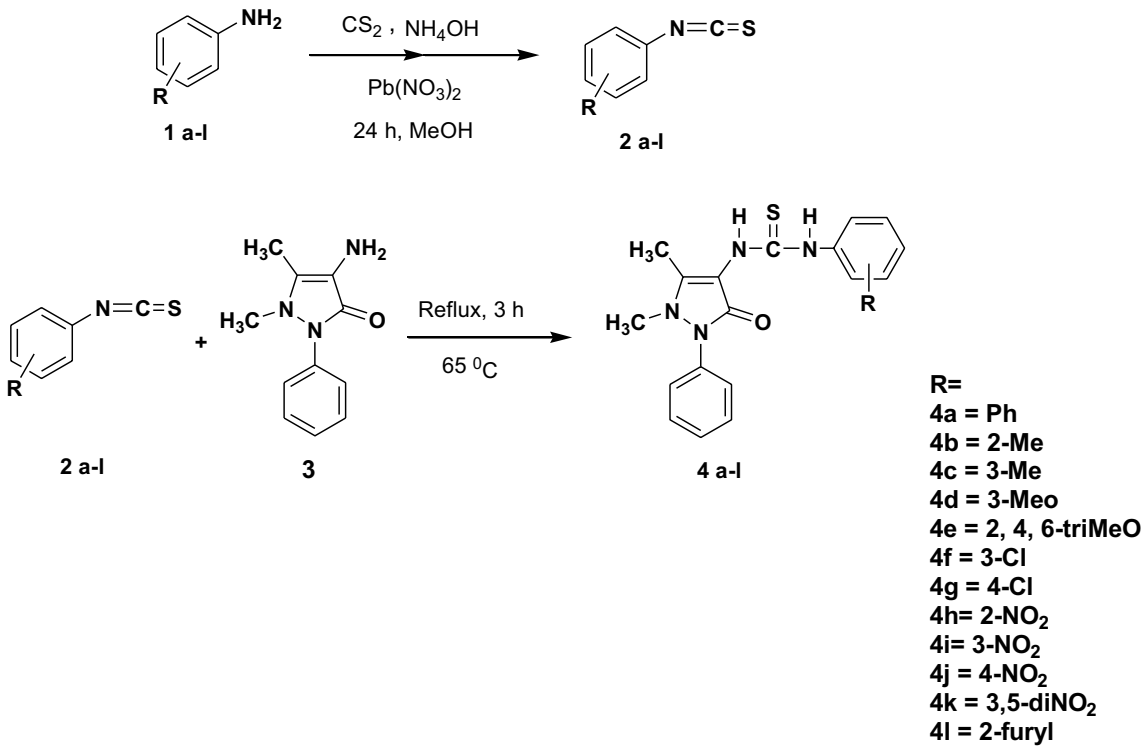

Scheme 1 Synthesis of substituted 1-(1,5-dimethyl-3-oxo-2-phenyl-2,3-dihydro-1*H*-pyrazol-4-yl)-3-phenylthioureas **(4a–l)**

while the stretching in the region ranging between 1267 and 1229 cm^{-1} is indicative of C=S bond of thiourea functionality. Additional absorption band in the region of 1703–1685 cm^{-1} highlights the C=O stretching of the 4-aminophenazone nucleus, whereas the presence of unsaturation in the structure is supported by the appearance of medium intensity signal around 3155–3027 cm^{1}, respectively.

The ^{1}H-NMR of synthesized compounds **4a–l** exhibits its dominant signals in the range of 11.72–9.05 ppm and 8.91–7.47 ppm which are indicative of N–H attached to substituted phenyl and to pyrazolone ring of 4-aminophenazone, respectively. The resonances in the form of singlet characteristic of the methyl groups, one in the downfield region due to the direct attachment with *aza* hetero atom, while the other slightly shifted toward shielding region, confirmed the presence of 4-aminophenazone moiety in the structure. The ^{13}C-NMR further supports the structure of synthesized compounds **4a–l** by showing resonances in the range of 189.1–181.4 ppm for the thiocarbonyl carbon besides other signals. The purity of newly prepared compounds is also ascertained by elemental analysis.

In vitro biological assays

Alkaline phosphatase assay

Activity of calf intestinal alkaline phosphatase (CIALP) was measured by spectrophotometric assay as described by Ashraf et al. [40] The entire assay experiments were repeated three times. KH_2PO_4 was used as the reference inhibitor of calf IALP in addition to L-phenylalanine that has been used for comparison as organic reference standard for IAP inhibition [41]. The results are summarized in Table 1.

The careful observation of the activity results, in terms of inhibition concentration (IC_{50}), reveals that several compounds of the series possess potent alkaline phosphatase inhibition activity which is much better than the reference standards used. Compound **4c** appears to be the most active member of the series with an IC_{50} value of 0.4 ± 0.01 µM. This increased activity, possessed by **4c**, is attributed to the presence of electron-donating group, i.e., the methyl group at meta-position in phenyl ring (Fig. 2). Second higher inhibition ($IC_{50} = 1.2 \pm 0.03$ µM) is shown by the **4g** member just by switching the substitution position from meta to para-position and nature of substituent from alkyl to halo group, respectively. Slight modification in the substitution pattern of halo group from para- to meta-position results in significant loss of activity (**4f** = $IC_{50} = 4.8 \pm 0.3$ µM). However, the presence of alkoxy group at meta-position leads to enhanced inhibition activity as shown by **4d** with $IC_{50} = 1.7 \pm 0.05$, while increasing substitution (poly-substitution) with polar alkoxy groups leads to significant loss of activity as observed in the case of **4e** (8.3 ± 0.2), thus making it least active member among the series. It was further encountered that reduction in carbon number of molecular skeleton is also linked with reduced inhibition as observed for unsubstituted phenyl derivative (**4a**: 4.8 ± 0.1) and for five-membered furyl-substituted derivative (**4l:** $IC_{50} = 5.0 \pm 0.09$), respectively. In a nutshell, the inhibition profile of the synthesized screened series **4a–l** features the importance of meta- and para-position for possessing good inhibition potential (Table 1).

Table 1 Alkaline phosphatase inhibition of 4-aminophenazone-derived aryl thiourea derivatives **(4a–l)**

Compound	$IC_{50} \pm$ SEM (µM)
4a	4.8 ± 0.1
4b	2.3 ± 0.07
4c	0.4 ± 0.01
4d	1.7 ± 0.05
4e	8.3 ± 0.2
4f	4.8 ± 0.3
4g	1.2 ± 0.03
4h	3.7 ± 0.1
4i	5.4 ± 0.1
4j	1.7 ± 0.051
4k	4.2 ± 0.2
4l	5.01 ± 0.09
KH_2PO_4	2.8 ± 0.06
L-Phenylalanine	100 ± 3.1

Values are presented as mean ± SEM

Standard error of mean

Kinetic studies

Based on IC_{50} value, the most potent inhibitor **4c** was selected to determine the mechanism of enzyme inhibition. The inhibitor concentrations used were 0.0, 0.100, 0.200 and 0.400 µM. Substrate *p*-NPP concentrations were 10, 5, 2.5, 1.25 and 0.625 mM. Pre-incubation time and other conditions were same as described in alkaline phosphatase inhibition assay section. Maximal initial velocities were determined from initial linear portion of absorbance up to 10 min, after addition of enzyme, at per min interval. The inhibition type on the enzyme was assayed by Lineweaver–Burke plot of inverse of velocities (1/V) versus inverse of substrate concentration 1/[S] mM^{-1} (Fig. 3). The EI dissociation constant K_i was determined by secondary plot of 1/V versus inhibitor concentration (Fig. 4).

The results presented in Table 2 indicate that the compound **4c** was determined to be non-competitive inhibitor of calf intestinal alkaline phosphatase. The inhibition constant K_i (0.360) was determined from Fig. 4. The value of $1/V_{max}$ is increased to a new value, while that of K_m remains same

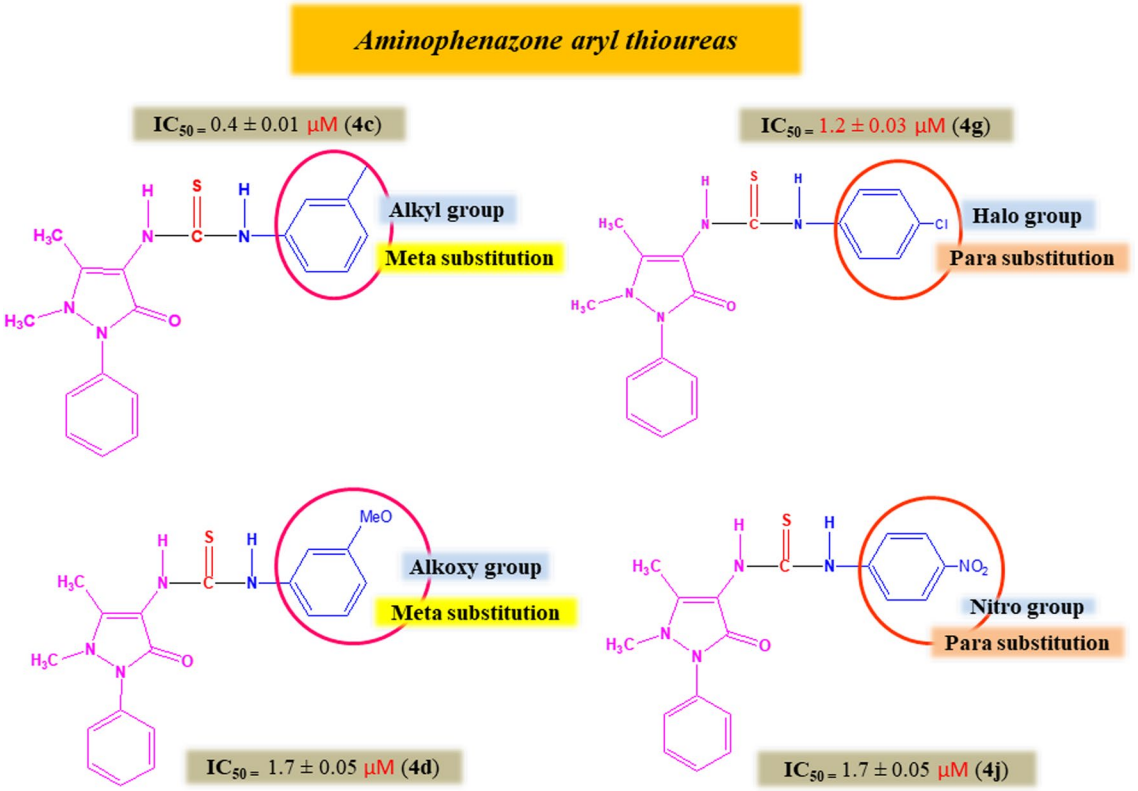

Fig. 2 Structure–activity relationship of some potent aminophenazone-derived aryl thioureas

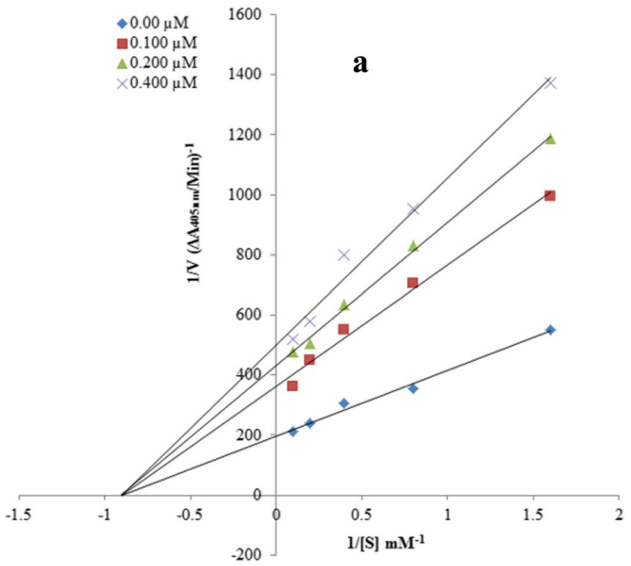

Fig. 3 Lineweaver–Burke plot

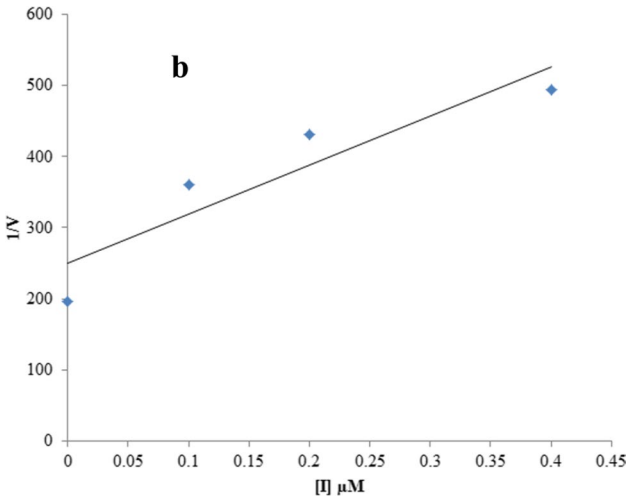

Fig. 4 Plot for determination of dissociation constant K_i

which indicated that compound **4c** simply lowers the concentration of enzyme by a non-competitive binding mode (Figs. 3, 4).

Toxicity evaluation using brine shrimp assay

The brine shrimp assay carried out for the synthesized compounds **(4a–l)** using potassium dihydrogen phosphatase as reference standard in terms of lethal doses is tabulated in Table 3.

Table 2 Kinetic analysis of compound **4c**

Entry	Concentration (μM)	$1/V_{max}$ (ΔA/Min)	K_m mM	K_i (μM)	Inhibition type
1	0.00	200.00	1.0952	0.360	Non-competitive
2	0.100	363.63	1.0952	0.360	
3	0.200	436.36	1.0952	0.360	
4	0.400	500.00	1.0952	0.360	

$1/V_{max}$ is the inverse of reaction velocities, K_m is the Michaelis–Menten constant, K_i is the inhibition constant

Table 3 LD_{50} of 4-aminophenazone-derived aryl thiourea derivatives **(4a–l)** engaging brine shrimp assay

Compound	LD_{50} (μM)
4a	70.9 ± 5.3
4b	90.4 ± 6.4
4c	84.1 ± 7.6
4d	85.2 ± 8.1
4e	112.5 ± 9.7
4f	110.2 ± 10.2
4g	115.4 ± 7.8
4h	121.4 ± 10.2
6i	125.2 ± 10.5
4j	95.467 ± 9.45
4k	106.7 ± 9.8
4l	87.9 ± 7.1
KH_2PO_4	89.1 ± 0.01

The results indicate that compound **4a** of the series, devoid of any substituent, turned out to be a lead candidate with $LD_{50} = 70.9 \pm 5.3$ μM, hence depicting that our compound is non-toxic up to 70 μM and thus is more safer compared to potassium dihydrogen phosphate. Further, in the series, the good LD_{50} is shown by derivatives **4c** and **4d** highlighting the significance of meta substitution with electron-donating groups, whereas switching the nature of substituent group from electron donating to electron withdrawing at meta-position, i.e., **4i,** results in total loss of activity with LD_{50} of 125.2 ± 10.5 μM.

Chemico-physical properties and RO5 validation of compound 4a–l

The basic chemico-physical properties of the synthesized compounds (**4a–l)** were predicted by using various *in silico* tools. The predicted properties like mol. wt. (g/mol), molar refractivity (cm^3), PSA ($Å^2$) and RO5 values of all synthesized compounds are listed in Table 4. It has been studied that drug properties such as molar refractivity and molecular lipophilicity are significant in receptor binding, bioavailability and cellular uptake. Moreover, PSA value is also very helpful parameter for drug absorption prediction in drug discovery [42]. Literature study is reported the standard values for molar refractivity and mol. wt. (40–130 cm^3) and (160–480 g/mol), respectively [43, 44]. The comparative analyses revealed that the predicted values of all the synthesized compounds were comparable with standard values. Moreover, irrespective of their higher mol. wt. (g/mol) and molar refractivity (cm^3) values, they showed very good drug likeness score. Moreover, RO5 analysis also justified the therapeutic potential of synthesized compounds. Literature study showed that hydrogen-bonding affinity has been considered as a significant parameter for evaluating the drug permeability [45]. It was observed that exceeded values of HBA (> 10) and HBD (> 5) in ligands results in poor permeation in the body. Our chemo-informatics analyses showed that all compounds possess < 10 HBA and < 5 HBD which may confirm their good penetration within the body. Moreover, their log *P* value was also comparable with standard values < 5. However, there are plenty of examples available for RO5 violation among the existing drugs [46].

Molecular docking analysis

Structural evaluation of target protein

Alkaline phosphatases (EC 3.1.3.1) are one of the most ubiquitous enzyme families processing phosphate groups [47]. Alkaline phosphatase exhibits 484 residues with single chain. Two zinc metal ions (Zn^{+2}) and magnesium ions

Table 4 Chemico-physical property of synthesized compounds (**4a–l)**

Properties	4a	4b	4c	4d	4e	4f	4g	4h	4i	4j	4k	4l
Mol. wt (g/mol)	338.12	352.14	352.14	368.14	428.15	372	372	384.11	384.11	384.11	430.12	328.10
No. HBA	2	2	2	3	5	2	2	4	4	4	6	3
No. HBD	2	2	2	2	2	2	2	3	3	3	4	2
Mol. Log P	2.7	3.3	3.1	3.84	2.78	3.46	3.46	2.22	2.34	2.34	1.94	1.78
Mol. PSA (A^2)	39.44	38.74	39.44	46.99	60.85	39.44	39.44	76.71	77.70	77.70	115.97	48.77
Mol. vol (A^3)	351.84	372.58	372.85	383.76	448.53	369.11	369.03	383.21	382.11	382.04	412.46	338.04
MR (cm^3)	98.95	103.5	103.5	105.31	118.04	103.7	103.7	104.98	104.98	104.98	111.01	91.43

**MR* molar refractivity

(Mg^{+2}) are also present in the active position within the protein (Fig. 5). However, calcium ions are also part of target protein [48]. The presence of these metals within the active region of target protein has a significant role in the downstream signaling pathways. The Ramachandran graph values depict the accuracy of phi (φ) and psi (ψ) angles among the coordinates of targeted protein. The predicted graph value showed that 98.1% residues were present in favored and 99.8% are part of allowed region. The predicted Ramachandran graph and hydrophobicity graphs are mentioned in supplementary data (Fig. S1a, b).

Binding energy evaluation of synthesized compounds

Docking experiment was employed to predict the best fitted conformational pose of synthesized ligands against alkaline phosphatase. The generated docked complexes were inspected on the basis of minimum docking energy values (Kcal/mol). The predicted docking results justified that compounds **4c** and **4g** exhibited a good binding energy values (− 10.30 and − 10.10 kcal/mol), respectively. However, all the other ligand also has good energy values. The binding energy value depicts the best conformational position within the active region of target protein. Although the basic nucleus of all the compounds is same, therefore, most of compounds possess good efficient and less fluctuated energy values (Fig. 6).

Binding pocket analysis of alkaline phosphatase and structure–activity relationship

Docked complexes were further evaluated on binding interactions (hydrogen or hydrophobic) of synthesized compounds against receptor protein. The ligands–protein binding analyses showed that most of compounds confined in the active binding region of target protein. The **4c** and **4g** were shown the best conformational state within the active binding site of alkaline phosphatase. Figures 7 and 8 show that **4c** forms four hydrogen bonds at Ser92 and His320 residues, while **4g** forms three hydrogen bonds with Ser92, His317 and His320 residues. One π–π stacking interaction was also observed at His317 with ligand benzene ring. The structure–activity relationship (SAR) study showed that carbonyl amino group of **4c** forms hydrogen bond with Ser92 at a distance 2.93 Å. While 5-membered cyclic oxygen of **4c** forms hydrogen bonds with His320 at a distance 2.98 Å in **4g**-docking complex, the 5-membered cyclic oxygen of **4g** ligand interacts by hydrogen bond with His320 having binding distance 2.65 Å, whereas the carbonyl sulfur moiety also form an hydrogen bond with His317 with a distance 2.99 Å. The benzene ring of ligand comes closer to benzene ring of

Fig. 5 Crystal structure of human alkaline phosphatase

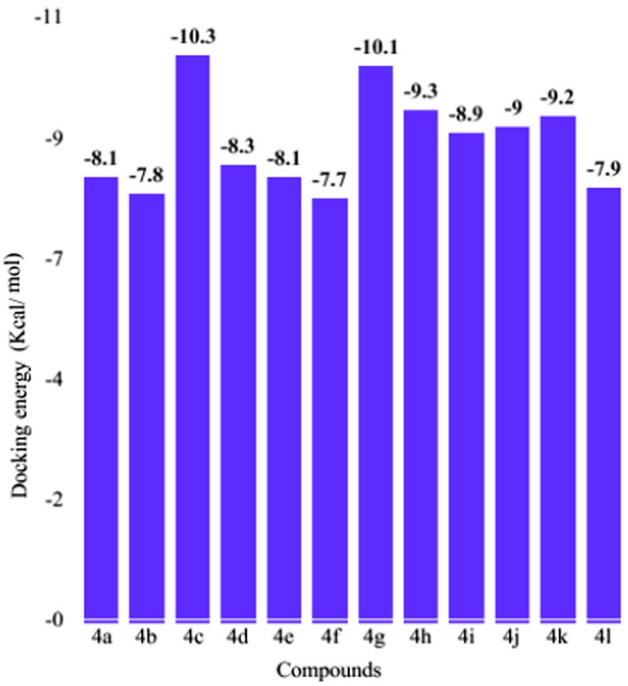

Fig. 6 Docking energy values

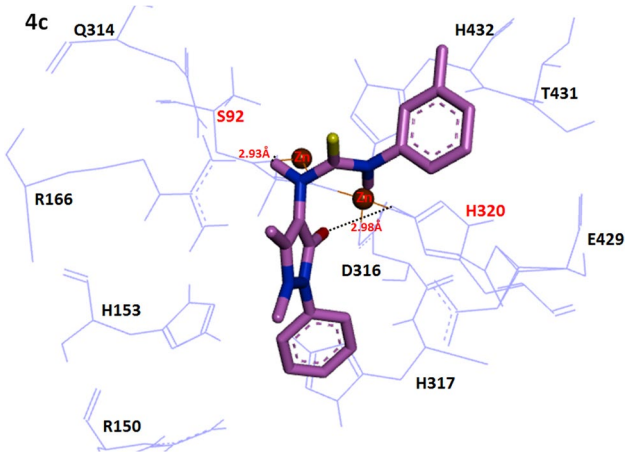

Fig. 7 Docking interaction of **4c** with target protein. The ligand is mentioned with purple color, while the functional groups like amino, sulfur and oxygen are highlighted with dark blue, yellow and red colors, respectively. The receptor protein residues are depicted light sky-blue color in wire format. The red dotted lines justify the hydrogen binding with distance mentioned in angstrom (Å). The red color residues show the interacted residues with ligand

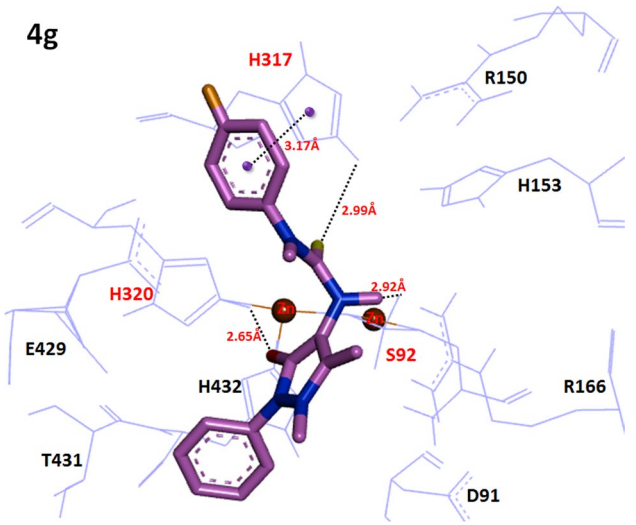

Fig. 8 Docking interaction of **4g** with target protein. The ligand is mentioned with purple color, while the functional groups like amino, sulfur and oxygen are highlighted with dark blue, yellow and red colors, respectively. The receptor protein residues are depicted light sky-blue color in wire format. The red dotted lines justify the hydrogen binding with distance mentioned in angstrom (Å). The red color residues show the interacted residues with ligand

His317 and forms the π–π staking interactions having distance 3.17 Å. Another hydrogen bond was observed between carbonyl amino group and Ser92 having bonding distance 2.92 Å. The SAR interpretation showed that oxygen and amino moieties are more significant and directly involves in the hydrogen-bonding interactions in active residues of target protein. It was interesting that His320 and Ser92 were common residues which bind with both compounds. Literature study reveals that Ser92 is the active binding residue of target protein and our synthesized compounds directly interact with this residue by making hydrogen bonds. The comparative results show that our docking results may be good agreement with active site of target protein. The energy values and hydrogen bindings of **4c** and **4g** showed their significance over other synthesized compounds. Moreover, computational results also show good correlation with assay studies. The graphical depictions of binding interactions of all the pro-drugs are mentioned in supplementary data (Figs. S2–S11).

Molecular dynamic simulations

Root mean square deviation and fluctuation (RMSD/RMSF) analysis of targeted protein

Based on docking results, **4c** and **4g** docking complexes selected to evaluate the residual flexibility of receptor molecule through MD simulation at 15 ns. The RMSD and RMSF graphs were assessed to determine the protein structural behavior in docking. Figure 9 shows the RMSD results of both **4c** and **4g** complexes which interprets the protein residual deviation and fluctuations in 15 ns simulation time frame. Initially, both graph lines were displayed an increasing trend from 0 to 2500 ps. The **4c** complex showed higher fluctuations than the **4g** at starting simulation time and depicts RMSD value 0.3 nm, while **4g** at 2500 ps time showed 0.25 nm. From 2500 to 5000 ps the **4c** complex remains stable, while **4g** showed increasing trends of fluctuations. After that, both **4c** and **4g** graph lines remain stable

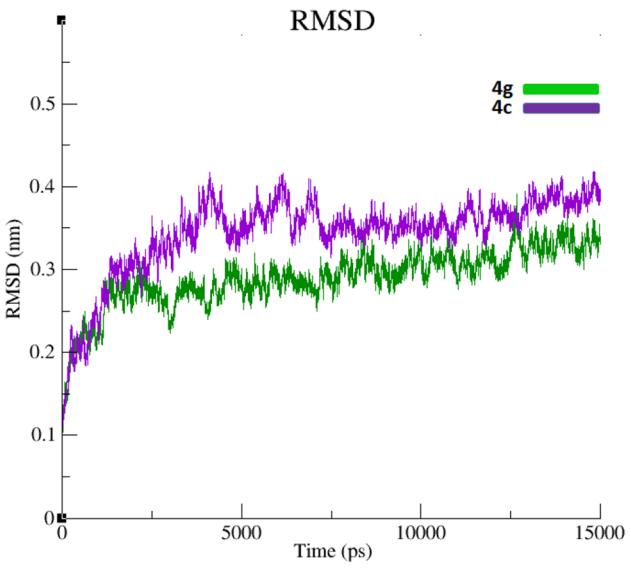

Fig. 9 RMSD graph of **4c** and **4g** docked complexes is mentioned in purple and green colors from 0 to 15,000 ps time scale

and showed little fluctuations throughout the simulation (5000–15,000 ps). The comparative analysis justified that **4g** complex simulation graph is little bit more stable throughout the simulation time period as compared to **4c** complex. However, their RMSD value has not too much deviant from each other. The generated RMSF results of both **4c** and **4g** complexes were shown the C and N-terminal lobes fluctuations of target protein throughout the simulation period. The generated graph showed that C-terminal loop region is much fluctuated. Result depicted that higher peaks in RMSF graph showed the loop conformation and its fluctuations in the simulation time (Fig. 10). The RMSF results assured the stability of **4c** and **4g** against targeted protein throughout the simulation period.

Radius of gyration (Rg) and solvent-accessible surface area (SASA) (A^2) prediction

Furthermore, radius of gyration (Rg) and solvent-accessible surface area (SASA) (A^2) were also keenly focused to analyze the compactness of target protein. The generated results exposed that Rg value is stable at 2.25 nm values throughout the simulation time frame 0–15,000 ps. The Rg time graph showed that residual backbone and folding of receptor protein were steadily stable after binding the inhibitors (Fig. 11). The solvent-accessible surface area (SASA) results showed that both complexes co-reside at 235 nm^2 in the simulations graphs (Fig. 12).

Conclusion

In the current research, a nonsteroidal anti-inflammatory drug "antipyrine" is synthetically modified to its substituted arylthiourea derivatives and screened against calf intestinal alkaline phosphatase for investigating their inhibition capacity for inflammation disorders. Results showed compounds **4c** and **4g** as lead inhibitors of the series with much enhanced IC_{50} than reference standards used. A most probable structure–activity relationship is anticipated by observing varying degree of inhibitory potential given by compounds **4a–l** that highlighted the significance of

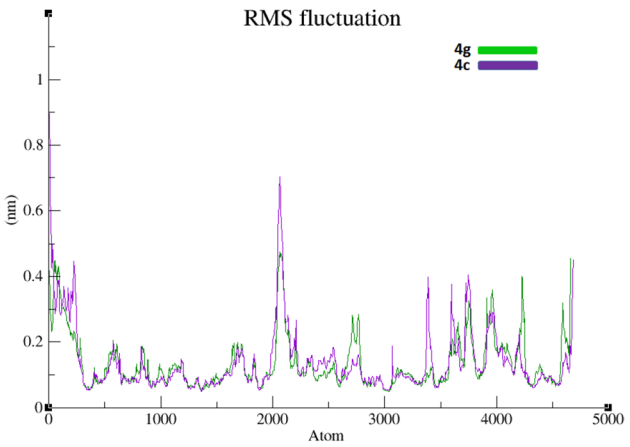

Fig. 10 RMSF graph of **4c** and **4g** docked complexes is mentioned in purple and green colors from 0 to 15,000 ps time scale

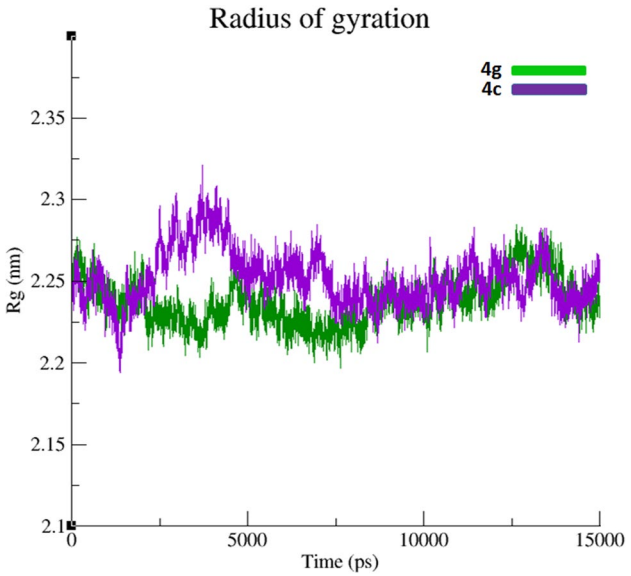

Fig. 11 Radius of gyration (Rg) graph of **4c** and **4g** docked complexes is mentioned in purple and green colors from 0 to 15,000 ps time scale

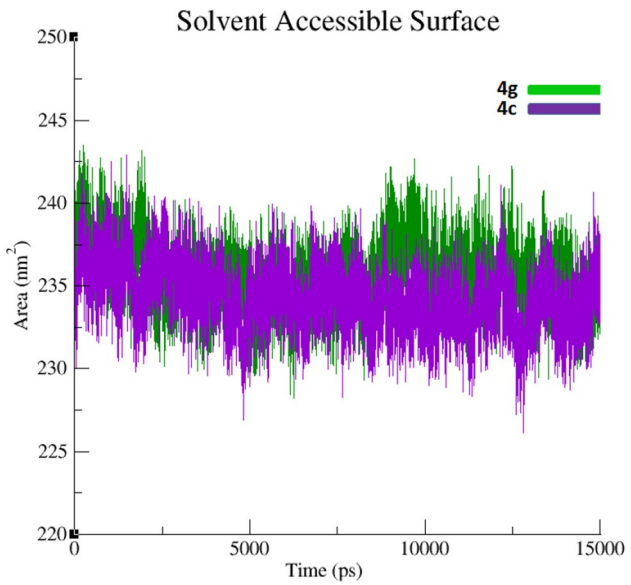

Fig. 12 Solvent-accessible surface area (SASA) graph of **4c** and **4g** docked complexes is mentioned in purple and green colors from 0 to 15000 ps time scale

meta-position in addition to para for enhanced inhibition profile, while molecular insights regarding the binding mode of aminophenazone thiourea analogs **4a–l** within the active pocket of alkaline phosphatase enzyme are rationalized by molecular docking studies and further supplemented by molecular dynamic simulations for the lead members **4c** and **4g**. Kinetic studies revealed that newly synthesized potent inhibitor **4c** binds to alkaline phosphatase via non-competitive fashion. RO5 validation of the synthesized derivatives is accomplished in addition to toxicity evaluation that justified their therapeutic potential.

Materials and methods

Experimental

Melting points were determined using Gallenkamp melting point apparatus (MP-D) and are uncorrected. Infrared spectra were recorded using a Bruker Tensor 27 FTIR spectrometer in ATR mode as neat samples. ^{1}H-NMR spectra were obtained using a Bruker 300 NMR MHz spectrometer in $CDCl_3$solution using TMS as an internal reference. ^{13}C-NMR spectra were obtained by (75 MHz) NMR spectrometer in deuterated solvents. Thin layer chromatography was performed on pre-coated silica gel aluminum plates (layer thickness 0.2 mm, HF 254, Riedel-de-Haen from Merck). Chromatogram was detected by using ultraviolet light (254 and 260 nm). MS was recorded using an EI source of (70 eV) on Agilent technologies 6890 N (GC) and an inert mass selective detector 5973 mass spectrometer. Elemental analyses were conducted using a LECO CHNS 932 instrument.

General procedure for the synthesis of substituted 1-(1,5-dimethyl-3-oxo-2-phenyl-2,3-dihydro-1*H*-pyrazol-4-yl)-3-phenylthioureas (4a–l)

To the solution of substituted aniline **1a–l** (0.1 g, 1.0 mmol) in methanol, carbon disulfide (0.06 mL, 1.0 mmol) and ammonium hydroxide (0.03 mL, 1.0 mmol) were added slowly at 10 °C followed by stirring for 12 h. Aqueous solution of lead nitrate is added to above mixture with additional stirring of 24 h to form isothiocyanates **2a–l,** that were purified via steam distillation to get rid of lead sulfide. The freshly synthesized isothiocyanates (**2a–l)** were then refluxed with solution of 4-aminophenazone **3** (0.2 g, 1.0 mmol) in acetone for **4h** to form the corresponding pure aryl thioureas **4a–l** after recrystallization from aqueous ethanol in good yields.

1-(1,5-Dimethyl-3-oxo-2-phenyl-2,3-dihydro-1*H*-pyrazol-4-yl)-3-phenylthiourea (4a)

Yellow amorphous solid; Yield: 80%; R_f: 0.47 (*n*-Hexane: $CHCl_3$, 4:1); m.p.: 67–68 °C; FTIR (ATR, cm^{-1}): 3358, 3250 (N–H), 1231 (C=S), 3153 (C^2_{SP}-H), 1685 (C=O); ^{1}H-NMR ($CDCl_3$, 300 MHz): δ 11.54 (s, 1*H*, NH-Ar), 9.96 (s, 1*H*, NH-pyrazole), 7.60–7.52 (m, 4*H*, Ar–H), 7.41–7.28 (m, 3H, Ar–H), 3.42 (s, 3H, $-NCH_3$), 2.96 (s, 3H, CH_3–Csp^2); ^{13}C-NMR ($CDCl_3$, 75 MHz): δ 189.7 (C=S), 161.9 (C=O pyrazole), 156.2, 155.5, 147.8, 145.8, 132.2, 130.1, 130.0, 127.8, 116.9, 112.2, 107.56, 37.6, 24.8. Anal. Calc. for $C_{18}H_{18}N_4OS$: C 63.85, H 5.39, N 16.69, S 9.40; Found: C 63.81, H 5.43, N 16.73, S 9.30.

1-(1,5-Dimethyl-3-oxo-2-phenyl-2,3-dihydro-1*H*-pyrazol-4-yl)-3-*o*-tolylthiourea (4b)

White amorphous solid; Yield: 80%; R_f: 0.42 (*n*-Hexane: $CHCl_3$, 4:1); m.p.: 89–90 °C; FTIR (ATR, cm^{-1}): 3348, 3230 (N–H), 1238 (C=S), 3128 (C^2_{SP}-H), 1700 (C=O); ^{1}H-NMR ($CDCl_3$, 300 MHz): δ 10.27 (s, 1*H*, NH-Ar), 9.38 (s, 1*H*, NH-pyrazole), 7.60–7.52 (m, 5H, Ar–H), 7.41–7.28 (m, 4*H*, Ar–H), 3.60 (s, 3H, $-NCH_3$), 3.40 (s, 3H, Ar-CH_3), 2.96 (s, 3H, CH_3-Csp^2); ^{13}C-NMR ($CDCl_3$, 75 MHz): δ 184.9 (C=S), 166.1 (C=O pyrazole), 148.3, 137.3, 129.9, 127.6, 126.7, 122.0, 121.1, 120.3, 34.7, 26.3, 19.2. Anal. Calc. for $C_{19}H_{20}N_4OS$: C 64.57, H 5.90, N 15.84, S 9.10; Found: C 64.51, H 5.96, N 15.94, S 9.00.

1-(1,5-Dimethyl-3-oxo-2-phenyl-2,3-dihydro-1*H*-pyrazol-4-yl)-3-*m*-tolylthiourea (4c)

Yellow crystalline solid; Yield: 79%; R_f: 0.41 (*n*-Hexane: $CHCl_3$, 4:1); m.p.: 74–75 °C; FTIR (ATR, cm^{-1}): 3343, 3215 (N–H), 1229 (C=S), 3141 (C^2_{SP}-H), 1701 (C=O); ^{1}H-NMR ($CDCl_3$, 300 MHz): δ 10.90 (s, 1*H*, NH-Ar), 9.51 (s, 1*H*, NH-pyrazole), 7.92–7.87 (m, 5H, Ar–H), 7.54–7.28 (m, 4*H*, Ar–H), 3.65 (s, 3H, $-NCH_3$), 3.42 (s, 3H, Ar-CH_3), 2.93 (s, 3H, CH_3-Csp^2); ^{13}C-NMR ($CDCl_3$, 75 MHz): δ 176.5 (C=S), 165.9 (C=O pyrazole), 140.0, 134.8, 134.4, 133.5, 133.2, 132.8, 132.0, 131.6, 128.4, 127.9, 127.1, 122.7, 121.6, 36.0, 28.0, 21.0. Anal. Calc. for $C_{19}H_{20}N_4OS$: C 64.51, H 5.96, N 15.94, S 9.20; Found: C 64.55, H 5.92, N 15.82, S 9.40.

1-(1,5-Dimethyl-3-oxo-2-phenyl-2,3-dihydro-1*H*-pyrazol-4-yl)-3-(3-methoxyphenyl)thiourea (4d)

Brown amorphous solid; Yield: 80%; R_f: 0.50 (*n*-Hexane: $CHCl_3$, 4:1); m.p.: 95–96 °C; FTIR (ATR, cm^{-1}): 3315, 3169 (N–H), 1247 (C=S), 3121 (C^2_{SP}-H), 1686 (C=O);

^{1}H-NMR ($CDCl_3$, 300 MHz): δ 11.11 (s, 1*H*, NH-Ar), 7.88 (s, 1*H*, NH-pyrazole), 7.78–7.20 (m, 5H, Ar–H), 6.98–6.86 (m, 5H, Ar–H), 3.45 (s, 3H, OCH_3), 3.25 (s, 3H, $-NCH_3$), 2.88 (s, 3H, CH_3-Csp^2); ^{13}C-NMR ($CDCl_3$, 75 MHz): δ 187.5 (C=S), 169.0 (C=O pyrazole), 160.2, 158.6, 139.8, 139.7, 137.9, 136.5, 130.4, 129.4, 128.9, 125.4, 125.3, 39.7, 37.7, 24.7. Anal. Calc. for $C_{19}H_{20}N_4O_2S$: C 61.52, H 5.99, N 15.44, S 8.60; Found: C 61.50, H 6.01, N 15.96, S 8.40.

1-(1,5-Dimethyl-3-oxo-2-phenyl-2,3-dihydro-1*H*-pyrazol-4-yl)-3-(2,4,6-tri-methoxyphenyl) thiourea (4e)

Yellow amorphous solid; Yield: 80%; R_f: 0.49 (*n*-Hexane: $CHCl_3$, 4:1); m.p.: 103–104 °C; FTIR (ATR, cm^{-1}): 3364, 3254 (N–H), 1261 (C=S), 3155 (C^2_{SP}-H), 1703 (C=O); ^{1}H-NMR ($CDCl_3$, 300 MHz): δ 11.56 (s, 1*H*, NH-Ar), 8.01 (s, 1*H*, NH-pyrazole), 8.08–7.60 (m, 5H, Ar–H), 7.58–7.29 (m, 2H, Ar–H), 4.05 (s, 9H, OCH_3), 3.72 (s, 3H, $-NCH_3$), 3.11 (s, 3H, CH_3-Csp^2); ^{13}C-NMR ($CDCl_3$, 75 MHz): δ 181.4 (C=S), 165.2 (C=O pyrazole), 146.3, 137.5, 128.4, 127.4, 124.6, 122.9, 120.5, 45.1, 38.5, 22.9. Anal. Calc. for $C_{21}H_{24}N_4O_4S$: C 58.36, H 6.15, N 13.00, S 7.35; Found: C 58.11, H 6.40, N 13.14, S 7.15.

1-(1,5-Dimethyl-3-oxo-2-phenyl-2,3-dihydro-1*H*-pyrazol-4-yl)-3-(3-chlorophenyl)thiourea (4f)

White amorphous solid; Yield: 81%; R_f: 0.45 (*n*-Hexane: $CHCl_3$, 4:1); m.p.: 116–117 °C; FTIR (ATR, cm^{-1}): 3263, 3213 (N–H), 1233 (C=S), 3027 (C^2_{SP}-H), 1688 (C=O); ^{1}H-NMR ($CDCl_3$, 300 MHz): δ 10.05 (s, 1*H*, NH-Ar), 8.47 (s, 1*H*, NH-pyrazole), 7.97–7.20 (m, 9H, Ar–H), 3.61 (s, 3H, $-NCH_3$), 2.20 (s, 3H, CH_3-Csp^2); ^{13}C-NMR ($CDCl_3$, 75 MHz): δ 187.4 (C=S), 166.9 (C=O pyrazole), 144.3, 135.1, 129.2, 126.6, 124.3, 123.9, 121.5, 35.4, 21.9. Anal. Calc. for $C_{18}H_{17}ClN_4OS$: C 57.95, H 4.63, N 15.14, S 8.74; Found: C 57.63, H 4.95, N 15.22, S 8.64.

1-(1,5-Dimethyl-3-oxo-2-phenyl-2,3-dihydro-1*H*-pyrazol-4-yl)-3-(4-chlorophenyl)thiourea (4g)

Yellow crystalline solid; Yield: 80%; R_f: 0.46 (*n*-Hexane: $CHCl_3$, 4:1); m.p.: 109–110 °C; FTIR (ATR, cm^{-1}): 3220, 3195 (N–H), 1239 (C=S), 3043 (C^2_{SP}-H), 1689 (C=O); ^{1}H-NMR ($(CD_3)_2SO$, 300 MHz): δ 11.14 (s, 1*H*, NH-Ar), 9.00 (s, 1*H*, NH-pyrazole), 7.71–7.68 (dd, 2H, Ar–H, 9 Hz, 6 Hz), 7.43–7.37 (dd, 2H, Ar–H, 9 Hz, 6 Hz) 6.99–6.94 (m, 5H, Ar–H), 3.57 (s, 3H, $-NCH_3$), 2.97 (s, 3H, CH_3-Csp^2); ^{13}C-NMR ($((CD_3)_2SO$, 75 MHz): δ 183.2 (C=S), 163.2 (C=O pyrazole), 159.1, 157.1, 146.0, 133.7, 131.2, 120.0, 118.6, 116.9, 38.1, 22.0. Anal. Calc. for $C_{18}H_{17}ClN_4OS$: C 57.90, H 4.66, N 15.10, S 8.70; Found: C 57.84, H 4.74, N 15.19, S 8.60.

1-(1,5-Dimethyl-3-oxo-2-phenyl-2,3-dihydro-1*H*-pyrazol-4-yl)-3-(2-nitrophenyl)thiourea (4h)

Brown amorphous solid; Yield: 78%; R_f: 0.44 (*n*-Hexane: $CHCl_3$, 4:1); m.p.: 131–132 °C; FTIR (ATR, cm^{-1}): 3329, 3239 (N–H), 1249 (C=S), 3119 (C^2_{SP}-H), 1692 (C=O); ^{1}H-NMR ($CDCl_3$, 300 MHz): δ 11.93 (s, 1*H*, NH-Ar), 9.79 (s, 1*H*, NH-pyrazole), 8.04–7.23 (m, 9H, Ar–H), 3.065 (s, 3H, $-NCH_3$), 2.37 (s, 3H, CH_3-Csp^2); ^{13}C-NMR ($CDCl_3$, 75 MHz): δ 187.3 (C=S), 166.2 (C=O pyrazole), 142.6, 138.1, 127.4, 126.9, 125.6, 124.9, 123.5, 37.3, 20.7. Anal. Calc. for $C_{18}H_{16}N_6O_5S$: C 56.33, H 4.52, N 18.15, S 8.23; Found: C 56.28, H 4.62, N 18.10, S 8.43.

1-(1,5-Dimethyl-3-oxo-2-phenyl-2,3-dihydro-1*H*-pyrazol-4-yl)-3-(3-nitrophenyl)thiourea (4i)

White amorphous solid; Yield: 79%; R_f: 0.40 (*n*-Hexane: $CHCl_3$, 4:1); m.p.: 121–122 °C; FTIR (ATR, cm^{-1}): 3378, 3234 (N–H), 1251 (C=S), 3079 (C^2_{SP}-H), 1697 (C=O); ^{1}H-NMR ($CDCl_3$, 300 MHz): δ 12.00 (s, 1*H*, NH-Ar), 10.29 (s, 1*H*, NH-pyrazole), 8.35–7.21 (m, 9H, Ar–H), 3.71 (s, 3H, $-NCH_3$), 2.41 (s, 3H, CH_3-Csp^2); ^{13}C-NMR ($CDCl_3$, 75 MHz): δ 189.1 (C=S), 167.2 (C=O pyrazole), 144.1, 138.1, 126.2, 125.0, 124.9, 123.2, 122.3, 38.6. 19.1. Anal. Calc. for $C_{18}H_{16}N_6O_5S$: C 56.37, H 4.50, N 18.28, S 8.23; Found: C 56.31, H 4.57, N 18.16, S 8.13.

1-(1,5-Dimethyl-3-oxo-2-phenyl-2,3-dihydro-1*H*-pyrazol-4-yl)-3-(4-nitrophenyl)thiourea (4j)

Yellow crystalline solid; Yield: 78%; R_f: 0.43 (*n*-Hexane: $CHCl_3$, 4:1); m.p.: 140–141 °C; FTIR (ATR, cm^{-1}): 3325, 3223 (N–H), 1236 (C=S), 3055 (C^2_{SP}-H), 1694 (C=O); ^{1}H-NMR ($(CD_3)_2O$, 300 MHz): δ 12.63 (s, 1*H*, NH-Ar), 10.48 (s, 1*H*, NH-pyrazole), 8.06–8.00 (m, 4*H*, Ar–H), 7.56–7.41 (m, 4*H*, Ar–H), 3.63 (s, 3H, $-NCH_3$), 2.56 (s, 3H, CH_3-Csp^2); ^{13}C-NMR ($(CD_3)_2O$, 75 MHz): δ 180.5 (C=S), 167.9 (C=O pyrazole), 133.6, 133.3, 132.2, 128.6, 128.3, 127.2, 126.5, 39.3, 18.2. Anal. Calc. for $C_{18}H_{16}N_6O_5S$: C 56.23, H 4.62, N 18.75, S 8.20; Found: C 56.30, H 4.57, N 18.13, S 8.36.

1-(1,5-Dimethyl-3-oxo-2-phenyl-2,3-dihydro-1*H*-pyrazol-4-yl)-3-(3,5-dinitrophenyl) thiourea (4k)

Pale yellow amorphous solid; Yield: 77%; R_f: 0.48 (*n*-Hexane: $CHCl_3$, 4:1); m.p.: 129–130 °C; FTIR (ATR, cm^{-1}):

3365, 3247 (N–H), 1258 (C=S), 3068 (C^2_{sp}-H), 1691 (C=O); ^{1}H-NMR ($CDCl_3$, 300 MHz): δ 12.70 (s, 1*H*, NH-Ar), 10.79 (s, 1*H*, NH-pyrazole), 8.18–7.26 (m, 7H, Ar–H), 3.94 (s, 3H, –NCH_3), 2.64 (s, 3H, CH_3-Csp^2); ^{13}C-NMR ($CDCl_3$, 75 MHz): δ 186.3 (C=S), 167.2 (C=O pyrazole), 143.31, 138.7, 137.5, 129.6, 126.6, 125.9, 122.7, 121.9, 39.6, 23.6. Anal. Calc. for $C_{18}H_{16}N_6O_5S$: C 50.36, H 3.86, N 19.64, S 7.45; Found: C 50.39, H 3.88, N 19.78, S 7.40.

1-(1,5-Dimethyl-3-oxo-2-phenyl-2,3-dihydro-1*H*-pyrazol-4-yl)-3-(furan-2-yl)thiourea (4l)

Brown amorphous solid; Yield: 81%; R_f: 0.51 (*n*-Hexane: $CHCl_3$, 4:1); m.p.: 147–148 °C; FTIR (ATR, cm^{-1}): 3375, 3228 (N–H), 1267 (C=S), 3082 (C^2_{sp}-H), 1699 (C=O); ^{1}H-NMR ($CDCl_3$, 300 MHz): δ 10.17 (s, 1*H*, NH-Ar), 8.41 (s, 1*H*, NH-pyrazole), 7.73–6.45 (m, 8H, Ar–H), 3.57 (s, 3H, –NCH_3), 2.43 (s, 3H, CH_3-Csp^2); ^{13}C-NMR ($CDCl_3$, 75 MHz): δ 188.7 (C=S), 166.2 (C=O pyrazole), 143.2, 136.7, 128.6, 128.1, 126.2, 111.3, 97.6, 37.5, 21.9. Anal. Calc. for $C_{16}H_{16}N_2O_2S$: C 58.50, H 4.93, N 17.59, S 9.76; Found: C 58.83, H 4.50, N 17.79, S 9.46.

Biological evaluation

Methodology of alkaline phosphatase assay

Activity of calf intestinal alkaline phosphatase (CIALP) was measured by spectrophotometric assay as previously described by [40]. The reaction mixture comprised of 50 mM Tris–HCl buffer (5 mM $MgCl_2$, 0.1 mM $ZnCl_2$ pH 9.5), the compound (0.1 mM with final DMSO 1% (v/v) and mixture was pre-incubated for 10 min by adding 5 µL of CIALP (0.025 U/mL). Then, 10 µL of substrate (0.5 mM *p*-NPP (para-nitrophenylphosphate disodium salt) was added to initiate the reaction and the assay mixture was incubated again for 30 min at 37 °C. The change in absorbance of released *p*-nitrophenolate was monitored at 405 nm, using a 96-well microplate reader (OPTI $_{MAX}$, Tunable USA). All the experiments were repeated three times in a triplicate manner. KH_2PO4 was used as the reference inhibitor of calf ALP.

Toxicity evaluation using brine shrimp assay

Culturing and harvesting of *Artemia salina*

Artemia salina cysts were incubated for hatching in a rectangular dish with a plastic divider with several holes making two uneven compartments. The container was filled with 3.3% solution of artificial seawater and dry yeast sprinkled into the larger compartment which was darkened. The smaller compartment was illuminated with light at 28 °C. After 24 h, hatched A. salina cysts were transferred to fresh artificial seawater and incubated for a further 24 h under artificial light and aeriation. The phototropic nauplii were collected by pipette from the lighted compartment.

Brine shrimps assay

A. salina nauplii (20) were counted macroscopically using Pasteur pipette against a lighted background and transferred into each sample vial and the solutions were made to 5 mL with test compound using serial dilutions with brine solution. A drop of dry yeast suspension was added as food to each vial. All the vials were maintained under light. The surviving nauplii were counted with the aid of a magnifying glass after 24 h. The mean mortality at the three dose levels for compound was determined and repeated thrice. Potassium dichromate was used as reference standard. After 24 h, the LD_{50} was calculated by probit analysis.

Compliance with ethical standards

Competing interest The authors declare that they have no known competing financial interests or personal relationships that could have appeared to influence the work reported in this paper.

References

1. Millan JL (2006) Mammalian alkaline phosphatases: from biology to applications in medicine and biotechnology. Wiley, Weinheim
2. Lalles JP (2010) Intestinal alkaline phosphatase: multiple biological roles in maintenance of intestinal homeostasis and modulation by diet. Nutr Rev 68:323–332
3. Lalles JP (2014) Intestinal alkaline phosphatase: novel functions and protective effects. Nutr Rev 72:82–94
4. Belli S, Sali A, Goding JW (1994) Divalent cations stabilize the conformation of plasma cell membrane glycoprotein PC-1 (alkaline phosphodiesterase I). Biochem J 304:75–80
5. Fleisch H, Bisaz S (1962) Mechanism of calcification: inhibitory role of pyrophosphate. Nature 195(911):911
6. Anderson HC, Hsu HH, Morris DC, Fedde KN, Whyte MP (1997) Matrix vesicles in osteomalacic hypophosphatasia bone contain apatite-like mineral crystals. Am J Pathol 151(15):55–61
7. Millan JL (2013) The role of phosphatases in the initiation of skeletal mineralization. Calcif Tissue Int 93:299–306
8. Altschul SF, Gish W, Miller W, Myers EW, Lipman DJ (1990) Basic local alignment search tool. J Mol Biol 215:403–410
9. Knapp K, Zebisch M, Pippel J, El-Tayeb A, Müller CE, Sträter N (2012) Crystal structure of the human ecto-5′-nucleotidase (CD73): insights into the regulation of purinergic signaling. Structure 20:2161–2173
10. Chen VB, Arendall WB, Headd JJ, Keedy DA, Immormino RM, Kapral GJ, Murray LW, Richardson JS, Richardson DC (2009) MolProbity: all-atom structure validation for macromolecular crystallography. Acta Crystallogr Sect D Biol Crystallogr 66:12–21

11. Sergienko EA, Millán JL (2010) High-throughput screening of tissue-nonspecific alkaline phosphatase for identification of effectors with diverse modes of action. Nat Protoc 5:1431–1439
12. Mahmood A, Engle MJ, Alpers DH (2002) Secreted intestinal surfactant-like particles interact with cell membranes and extracellular matrix proteins in rats. J Physiol 542(237):44
13. McConnell RE, Higginbotham JN, Shifrin DA, Tabb DL, Coffey RJ, Tyska MJ (2009) The enterocyte microvillus is a vesicle-generating organelle. J Cell Biol 185(12):85–98
14. Akiba Y, Mizumori M, Guth PH, Engel E, Kaunitz JD (2007) Duodenal brush border intestinal alkaline phosphatase activity affects bicarbonate secretion in rats. Am J Physiol Gastrointest Liver Physiol 293:1223–1233
15. Šefčíková Z, Hájek T, Lenhardt L, Racek L, Mozes S (2008) Different functional responsibility of the small intestine to high-fat/high-energy diet determined the expression of obesity-prone and obesity-resistant phenotypes in rats. Physiol Res 57(4):67–74
16. Barbier de La Serre C, Ellis CL, Lee J, Hartman AL, Rutledge JC, Raybould HE (2010) Propensity to high-fat diet-induced obesity in rats is associated with changes in the gut microbiota and gut inflammation. Am J Physiol Gastrointest Liver Physiol 299(2):G440–G448
17. Malo MS (2015) A high level of intestinal alkaline phosphatase is protective against type 2 diabetes mellitus irrespective of obesity. EBioMedicine 2:2016–2023
18. Kaliannan K, Hamarneh SR, Economopoulos KP, Alam SN, Moaven O, Patel P (2013) Intestinal alkaline phosphatase prevents metabolic syndrome in mice. Proc Natl Acad Sci USA 110:7003–7008
19. Sharma U, Pal D, Prasad R (2014) Alkaline phosphatase: an overview. Indian J Clin Biochem 29(3):269–278
20. Šali A, Blundell TL (1993) Comparative protein modelling by satisfaction of spatial restraints. J Mol Biol 234(3):779–815
21. Ghorab MM, El-Gaby MSA, Safwat NA, Elaasser MM, Soliman AM (2016) Biological evaluation of some new *N*-(2,6-dimethoxypyrimidinyl) thioureido benzenesulfonamide derivatives as potential antimicrobial and anticancer agents. Eur J Med Chem 124(29):299–310
22. Sjid ur Rehman, Saeed A, Saddique G, Channar PA, Laraik FA, Abbas Q, Hassan M, Raza H, Fattah TA, Seo SY (2018) Synthesis of sulfadiazinyl acyl/aryl thiourea derivatives as calf intestinal alkaline phosphatase inhibitors, pharmacokinetic properties, lead optimization, Lineweaver–Burk plot evaluation and binding analysis. Bioorg Med Chem 26(12):3707–3715
23. Marwa SY, El-Sharief AM, Basyouni WM, Fakhr IMI, El-Gammal EW (2013) Thiourea derivatives incorporating a hippuric acid moiety: synthesis and evaluation of antibacterial and antifungal activities. Eur J Med Chem 64:111–120
24. Li JP, Luo QF, Wang YL, Wang H (2001) Solvent-free synthesis of heterocyclic thioureas using microwave technology. J Chin Chem Soc 48(1):73–75
25. Glasser AC, Doughty RM (1962) Substituted heterocyclic thioureas I. Antitubercular activity. J Pharma Sci 51:1031–1033
26. Shah AC, Herd AK (1973) Pharmaceutical sciences—1972: literature review of pharmaceutics I. Egypt. J Pharmaceut Sci 14:214
27. Strukil V (2017) Mechanochemical synthesis of thioureas, ureas and guanidines. Beilstein J Org Chem 13:1828–1849
28. Ngaini Z, Zulkiplee WZHW, Halim ANA (2017) One-pot multicomponent synthesis of thiourea derivatives in cyclotriphosphazenes moieties. J Chem. https://doi.org/10.1155/2017/1509129
29. Štrukil V, Margetić D, Igrc MD, Eckert-Maksić M, Friščić T (2012) Desymmetrisation of aromatic diamines and synthesis of non-symmetrical thiourea derivatives by click-mechanochemistry. Chem Commun 48:9705–9707
30. Đud M, Magdysyuk OV, Margetić D, Štrukil V (2016) Synthesis of monosubstituted thioureas by vapour digestion and mechanochemical amination of thiocarbamoyl benzotriazoles. Green Chem 18:2666–2674
31. Li AF, Wang JH, Wang F, Jiang YB (2010) Anion complexation and sensing using modified urea and thiourea-based receptors. Chem Soc Rev 39:3729–3745
32. Bregović N, Cindro N, Frkanec L, Užarević K, Tomišić V (2014) Thermodynamic study of dihydrogen phosphate dimerisation and complexation with novel urea- and thiourea-based receptors. Chem A Eur J 20(48):15863–15871
33. Mumtaza A, Saeeda K, Mahmood A, Zaib S, Saeed A, Pelletier J, Sévigny J, Iqbal J (2010) Bisthioureas of pimelic acid and 4-methylsalicylic acid derivatives as selective inhibitors of tissue-nonspecific alkaline phosphatase (TNAP) and intestinal alkaline phosphatase (IAP): synthesis and molecular docking studies. Bioorg Chem 101:103996
34. Dharmasiri MG, Jayakody JRAC, Galhena G, Liyanage SSP, Ratnasooriya WD (2003) Anti-inflammatory and analgesic activities of mature fresh leaves of *Vitex negundo*. J Ethnopharmacol 87:199–206
35. Turan-Zitouni G, Sivaci M, Kiliç FS, Erol K (2001) Synthesis of some triazolyl-antipyrine derivatives and investigation of analgesic activity. Eur J Med Chem 36:685–689
36. Channar PA, Afzal S, Ejaz SA, Saeed A, Laraik FA, Mahesar PA, Lecka J, Sévigny J, Erben MF, Iqbal J (2018) Exploration of carboxy pyrazole derivatives: synthesis, alkaline phosphatase, nucleotide pyrophosphatase/phosphodiesterase and nucleoside triphosphate diphosphohydrolase inhibition studies with potential anticancer profile. Eur J Med Chem 5(156):461–478
37. Ayako K, Hidehiko N, Ryo O, Tomoko F, Shigeru O, Takayoshi S, Naoki M (2007) New series of antiprion compounds: pyrazolone derivatives have the potent activity of inhibiting protease-resistant prion protein accumulation. J Med Chem 50:5053–5056
38. Shyama S, Robert A, Ying S, Sonoko N, Brock B, José Luis M, Eduard S, Nicholas DPC (2009) Design and synthesis of pyrazole derivatives as potent and selective inhibitors of tissue-nonspecific alkaline phosphatase (TNAP). Bioorg Med Chem Lett 19:222–225
39. Aamer S, Syeda AE, Asma K, Sidra H, Mariya R, Muhammad L, Joanna L, Jean S, Iqbal J (2015) Synthesis, characterization and biological evaluation of *N*-(2,3-dimethyl-5-oxo-1-phenyl-2,5-dihydro-1*H*-pyrazol-4-yl)benzamides. RSC Adv 5(105):86428–86439
40. Ashraf Z, Rafiq M, Seo S-Y, Kwon K, Babar MM (2015) Kinetic and in silico studies of novel hydroxy-based thymol analogues as inhibitors of mushroom tyrosinase. Eur J Med Chem 98:203–211
41. Iqbal J, El-Gamal MI, Ejaz SA, Lecka J, Sevigny J, Ohg CH (2018) Tricyclic coumarin sulphonate derivatives with alkaline phosphatase inhibitory effects: in vitro and docking studies. J Enzyme Inhib Med Chem 33(1):479–484
42. Peter E, Bernhard R, Paul S (2000) Fast calculation of molecular polar surface area as a sum of fragment-based contributions and its application to the prediction of drug transport properties. J Med Chem 43:3714–3717
43. Ghose AK, Herbertz T, Hudkins RL, Dorsey BD, Mallano JP (2012) Knowledge-based, central nervous system (CNS) lead selection and lead optimization for CNS drug discovery. ACS Chem Neurosci 3:50–68
44. Kadam RU, Roy N (2007) Recent trends in drug-likeness prediction: a comprehensive review of in silico methods. Indian J Pharm Sci 69:609–615
45. Bakht MA, Yar MS, Abdel-Hamid SG, Al-Qasoumi SI, Samad A (2010) Molecular properties prediction, synthesis and antimicrobial activity of some newer oxadiazole derivatives. Eur J Med Chem 45:5862–5869
46. Tian S, Wang J, Li Y, Li D, Xu L, Hou T (2015) The application of in silico drug-likeness predictions in pharmaceutical research. Adv Drug Deliv Rev 86:2–10

47. Millán JL (2006) Alkaline phosphatases. Purinergic Signal 2(1):335–341
48. Stec B, Cheltsoy A, Millán JL (2010) Refined structures of placental alkaline phosphatase show a consistent pattern of interactions at the peripheral site. Acta Crystallogr Sect F Struct Biol Cryst Commun 66(1):866–870